Journal of Materials Chemistry A

Photolithographic p–n patterning of single-walled carbon nanotube sheets using photobase generators

Journal:	*Journal of Materials Chemistry A*
Manuscript ID	TA-ART-08-2023-005067.R1
Article Type:	Paper
Date Submitted by the Author:	04-Oct-2023
Complete List of Authors:	Tanaka, Naoki; Kyushu University, Applied Chemistry Yamamoto, Mei; Kyushu University, Applied Chemistry Yamaguchi, Itsuki; Kyushu University Hamasuna, Aoi; Kyushu University Honjo, Emi; Kyushu University, Applied Chemistry Fujigaya, Tsuyohiko; Kyushu Daigaku Kogakubu Daigakuin Kogakufu,

PAPER

Photolithographic p–n patterning of single-walled carbon nanotube sheets using photobase generators

Received 00th January 20xx,
Accepted 00th January 20xx

DOI: 10.1039/x0xx00000x

Naoki Tanaka,[ab] Mei Yamamoto,[a] Itsuki Yamaguchi,[a] Aoi Hamasuna,[a] Emi Honjo,[a] and Tsuyohiko Fujigaya*[abc]

Single-walled carbon nanotubes (SWCNTs) are promising thermoelectric materials because of their high electrical conductivity and Seebeck coefficient. To construct a thermoelectric generator (TEG) employing SWCNTs, the development of n-type regions within a single piece of p-type SWCNTs has gained interest, offering a seamless TEG structure without the need for metal electrodes to bridge the p- and n-type regions. Several patterning methods such as thermal deposition, plasma-induced degradation, and photoinduced doping have been put forward as potential substitutes for traditional drop casting owing to their straightforward processes and superior patterning resolution. In this study, a photobase generator (PBG) was utilized as an n-type dopant for photoinduced doping. The PBG-doped SWCNTs demonstrated exceptional thermal stability, retaining a p-type nature in the absence of UV irradiation, which, upon UV exposure, spontaneously transitioned to n-type. Moreover, the resulting n-doped region displayed remarkable stability in air for more than 100 days. Employing this technique, planar-type TEG devices with up to six p- and n-type regions in sequence were constructed. The TEGs exhibited an in-plane open-circuit voltage and maximum power output of 3.45 mV and 5.75 nW, respectively, when a temperature gradient of 30 °C was applied between the front and back sides of the sheets.

1. Introduction

The trend toward low-power-consumption electronic devices has highlighted the significance of energy harvesting techniques. Energy harvesting devices capture energy from the environment, transforming it into usable electrical power, and are finding applications in diverse areas, such as industrial automation, wireless sensors, and the Internet of Things (IoT).[1-5] Among these, thermoelectric generators (TEGs) stand out for their capacity to generate electricity from the thermal differences generated by heat sources such as factories, automobiles, and even the human body. This technology leverages the Seebeck effect, where a temperature gradient across a material generates voltage.[6-10]

Typical TEG devices adopt a "π-type" structure with alternating p- and n-type semiconductor regions in a zigzag arrangement, connected using metal or conductive paste.[11-16] This series structure produces an open-circuit voltage (V_{OC}):

$$V_{OC} = n(S_P - S_N)\Delta T \quad (1)$$

where n is the number of p–n units, S_P and S_N are the p- and n-type Seebeck coefficients, respectively, and ΔT is the

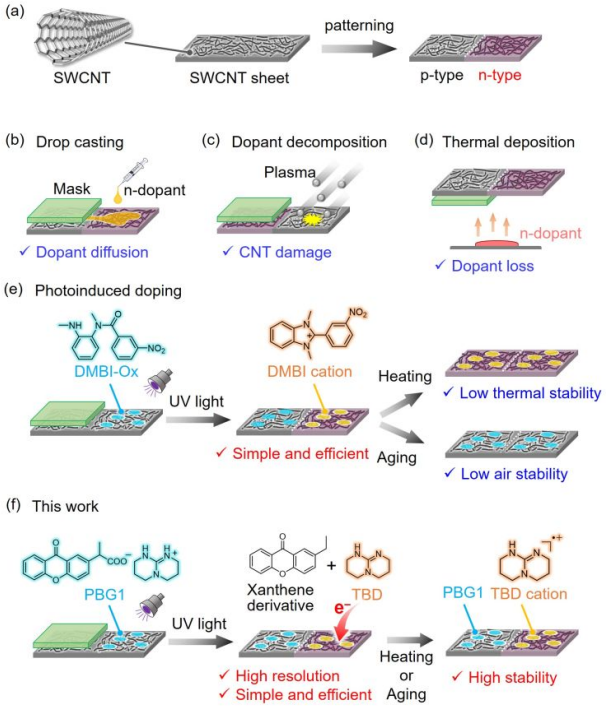

Fig. 1 (a) Schematic representation of p–n patterning of an SWCNT sheet through doping. Illustrations of established p–n patterning methodologies of SWCNT sheets, (b) drop casting, (c) dopant decomposition, (d) thermal deposition, and (e) photoinduced doping. (f) Conceptual framework for photoinduced electron doping of SWCNTs by UV irradiation of PBG1, as established in this study.

[a] Department of Applied Chemistry, Graduate School of Engineering, Kyushu University, 744 Motooka, Nishi-ku, Fukuoka 819-0395, Japan. E-mail: fujigaya.tsuyohiko.948@m.kyushu-u.ac.jp
[b] International Institute for Carbon Neutral Energy Research (WPI-I2CNER), 744 Motooka, Nishi-ku, Fukuoka 819-0395, Japan
[c] Center for Molecular Systems (CMS), 744 Motooka, Nishi-ku, Fukuoka 819-0395, Japan

†Electronic Supplementary Information (ESI) available: Additional spectroscopic data, Seebeck coefficient data. See DOI: 10.1039/x0xx00000x

temperature gradient across the material. Therefore, employing materials with high Seebeck coefficients and increasing the number of p–n units is advantageous for achieving high open-circuit voltages as well as high power factor (*PF*):

$$PF = S^2\sigma \quad (2)$$

where σ is the electrical conductivity.

Single-walled carbon nanotubes (SWCNTs) have emerged as promising materials for TEG devices owing to their excellent electrical conductivity, Seebeck coefficients, and notable physical properties like strength, thermal stability, flexibility, and processability.[17,18] SWCNTs are inherently n-type semiconductors, but they display p-type behavior by atmospheric oxidation. This instability has necessitated the development of stable n-doped SWCNTs. Several chemical n-type dopants such as polyethyleneimine,[19-21] benzimidazole derivatives,[22-26] crown ether salts,[27,28] and guanidine derivatives[29] have been reported. Using these n-type dopants, many SWCNT-based TEG devices with π-type structures have been developed.[17,18,30-32]

One challenge for improving the power generation of SWCNT-based TEGs is to reduce the contact resistance at the connections between the p- and n-type regions and the bridging materials. A potential solution is to fabricate joint-free TEG structures, wherein p- and n-type regions alternate on a single SWCNT sheet or fiber (i.e., p–n patterning) (Fig. 1a).

Drop casting is the simplest and most widely used method for p–n patterning, in which an n-type dopant solution is cast onto pristine SWCNTs (p-type) with the use of masking (Fig. 1b).[32-34] However, drop casting has poor patterning resolution (on the millimeter scale) because the dopant solution diffuses at the p–n boundaries due to capillary effects.[35] Dai et al. proposed a plasma treatment for p–n patterning that demonstrated a high patterning resolution (<5 μm) (Fig. 1c);[35] however, this method introduced sp^3 defects that decreased the electrical conductivity of the SWCNT sheets. Recently, we developed a method involving the thermal deposition of a p-type dopant precursor using a vacuum chamber to achieve p–n patterning with good resolution (<100 μm) (Fig. 1d).[23] However, this method required an excess of n-type dopant molecules and a long processing time.

Recently, we developed photopatterning of p-type SWCNT sheets based on a photochemical reaction of n-dopant precursor (DMBI-Ox: Fig. 1e) that achieved fine p–n patterns by UV irradiation (10 min) process with a photomask (Fig. 1e).[36] This method does not require any patterning of the dopant molecules but easily fabricates p-n patterns in arbitrary design without damaging the SWCNT structure. However, in this system, both an unirradiated p-type area and an irradiated n-type area faced the stability issue; namely, p-type area turned to n-type upon heating due to thermal activation of the DMBI-Ox (Fig. S1†) and the n-doped region was gradually turned to p-type under atmospheric condition within 20 days due to the oxidation of n-type SWCNT. Therefore, there is a need for a photolithographic patterning method that provides high thermal stability and high air stability.

To address this, we developed a new photoinduced n-type doping method using photobase generators (PBGs). PBGs produce organic bases upon UV irradiation and have been used for photolithography.[37-42] Since PBGs were thermally stable under the photolithography process that applied thermal treatment above 150 °C,[43] high thermal stability in the p-type area (unirradiated area) can be expected. Among PBGs, PBG1 was selected because it produces 1,5,7-triazabicyclo[4.4.0]dec-5-ene (TBD) under UV irradiation (λ_{ex} = 365 nm), which has been reported as a good n-type dopant for SWCNTs owing to its high basicity (electron-donating property) (Fig. 1f and Fig. S2†).[29,44] Horike et al. reported that TBD-doped SWCNTs showed high air stability even at 100 °C because of the stability of the TBD cation, along with the high coverage ratio of the TBD cation on the negatively charged n-doped SWCNT surface.[29] Wei et al. utilized PBG1 to control carrier concentration of poly(3,4-ethylenedioxythiophene)/poly(styrenesulfonate) by photoirradiation.[42] In this study, we successfully prepared n-doped SWCNT sheets using PBG1 by photoirradiation for 1 min and found that the resulting n-doped SWCNT sheets were thermally stable and showed good air stability for more than 100 days. We then created high-resolution p–n patterns in SWCNT sheets using photomasks, leading to the development of new TEG devices.

2. Experimental section

2.1 Materials

SWCNTs (Meijo-eDIPS) with an average diameter of 1.5 nm and 1.3 nm were purchased from Meijo Nano Carbon. SWCNT (CoMoCAT (6,5) rich) with an average diameter of 0.78 nm was purchased from Sigma-Aldrich Corporation. *N*-methylpyrrolidone (NMP), methanol, deuterated methanol, and several types of PBG [PBG2: 1,2-diisopropyl-3-[bis(dimethylamino)methylene]guanidium 2-(3-benzoylphenyl)propionate; PBG3: 1,2-dicyclohexyl-4,4,5,5-tetramethylbiguanidium n-butyltriphenylborate; and PBG4: (*Z*)-[[bis(dimethylamino)methylidene]amino]-*N*-cyclohexyl(cyclohexylamino)methaniminium tetrakis(3-fluorophenyl)borate] were purchased from FUJIFILM Wako Pure Chemicals Corp (Tokyo, Japan). PBG1 (2-(9-oxoxanthen-2-yl)propionic acid 1,5,7-triazabicyclo[4.4.0]dec-5-ene salt) was purchased from Tokyo Chemical Industry (Tokyo, Japan). A thermally insulating aerogel (1 mm thick) with a thermal conductivity of 0.016 W/mK was obtained from INOAC Corp (Aichi, Japan), and copper and gold wires were purchased from Nilaco Corporation (Tokyo, Japan).

2.2 Characterization

^{1}H NMR spectra were recorded at 25 °C using a JEOL JNM-ECZ400 spectrometer at 400 MHz. Raman spectra were recorded at an excitation wavelength of 533 nm using a Raman touch spectrometer (Nanophoton Corporation, Osaka, Japan). The in-plane electrical conductivity and in-plane Seebeck coefficient were determined using a ZEM-3 measurement system (ADVANCE RIKO, Yokohama, Japan) under helium and air atmospheres at temperatures of 30–100 °C. SWCNT sheets

(22 × 4 mm) mounted on a ceramic block (22 × 4 × 3 mm) were fixed with two Ni electrodes at both ends. Currents were flown between the electrodes, while the potential and temperature differences were measured using two thermocouples in the middle of the sheets. KFM was conducted using an SPM-9700HT instrument (Shimadzu, Kyoto, Japan), and the current–voltage (*I*–*V*) curves were analyzed using a Keithley 2401 source meter (Tektronix, Tokyo, Japan). The temperature of the SWCNT sheets was monitored using an InfReC R450 thermal imaging camera (Nippon Avionics Co., Ltd., Yokohama, Japan).

2.3 Fabrication of SWCNT sheets

SWCNTs (1.0 mg) were dispersed in NMP (40 mL) using a bath-type sonicator (Branson 5010) for 1 h. The dispersion was passed through a cotton-plugged Pasteur pipette to remove agglomerated SWCNTs. The filtered dispersion was then passed through a PTFE membrane (diameter: 90 mm, pore size: 0.2 µm) to form SWCNT sheets. Residual NMP was removed by dipping the sheets in methanol, followed by vacuum drying at 80 °C for 8 h. The sheet thickness was approximately 1.0 ± 0.2 µm.

2.4 Photoinduced electron doping of SWCNTs using PBGs

The SWCNT sheets on PTFE membranes were cut into 14 × 4 mm pieces and then immersed in a methanol solution of PBG1 for 1 h. Subsequently, the SWCNT sheets were vacuum-dried at room temperature for 24 h. Following this, UV light (50 mW/cm^2) was used to irradiate the PBG-doped SWCNT sheets for photoinduced electron doping. The thermoelectric properties of the photodoped SWCNT sheets were evaluated.

2.5 Fabrication of planar SWCNT-based TEGs

SWCNT sheets on PTFE membranes were cut into 10 × 50 mm pieces and similarly immersed in a methanol solution of PBG1 for 1 h. After immersion, the SWCNT sheets were vacuum-dried at room temperature for 24 h. Aluminum foil was used to mask the SWCNT sheets for p–n patterning during UV irradiation TEGs with one, two, four, and six p–n sequences were produced. Gold wires were connected to both ends of the SWCNT sheets using conductive paste. For selective heating at the p–n boundaries, Cu bars with dimensions of 0.3 × 10 mm were embedded in a thermally insulating sheets (30 × 50 × 1 mm) at the respective distances between the p–n junctions of each patterned SWCNT. The SWCNTs and Cu bars were bonded using a conductive paste, while thermal pastes were applied to the heater and Cu side to enhance heat transfer.

2.6 Theoretical calculations

The optimization and energy levels of counter cations in PBG1, PBG2, PBG3, and PBG4 were calculated using Gaussian 16 at the B3LYP/6-31G(d,p) level.

3. Results and discussion

3.1 Photoinduced Electron Doping of SWCNT by PBG1

Pristine SWCNT sheets were prepared by filtering an *N*-methylpyrrolidone (NMP) dispersion of SWCNTs using a polytetrafluoroethylene (PTFE) membrane. We then soaked the

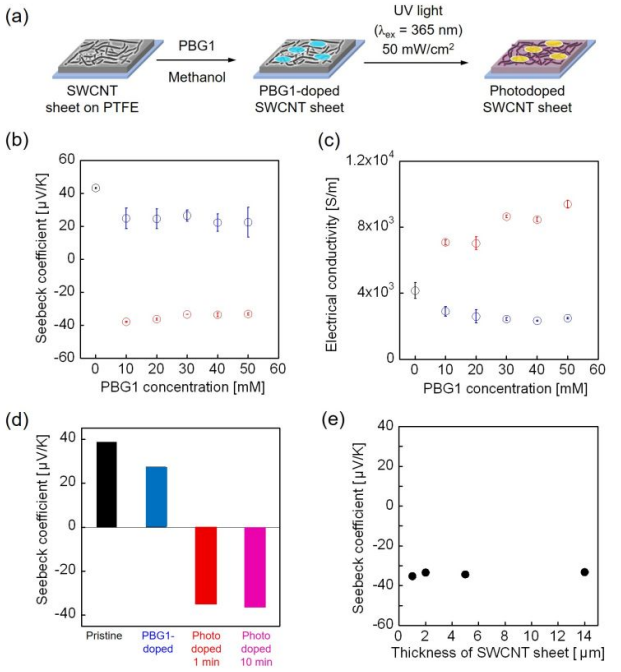

Fig. 2 (a) Procedure for the preparation of PBG1-doped SWCNT sheets and the subsequent photoinduced electron doping. (b) PBG1 concentration dependence of Seebeck coefficient and (c) electrical conductivity for pristine (black), PBG1-doped (blue), and photodoped (red) SWCNT sheets at 30 °C under a helium atmosphere. Error bars represent the standard deviation of three technical replicates. (d) Dependence of Seebeck coefficient on irradiation time for SWCNT sheets after immersion in a 30 mM PBG1 solution. e Dependence of Seebeck coefficient on thickness of SWCNT sheets after immersion in a 30 mM PBG1 solution and irradiation with UV light (λex = 365 nm) for 1 min. The 14 µm thick SWCNT sheet was irradiated for 30 min.

SWCNT sheets in a methanol solution of PBG1 (0–50 mM) for 1 h to prepare PBG1-doped SWCNT sheets, and subsequently exposed these sheets to UV light (λ_{ex} = 365 nm, 50 mW/cm^2) for 1 min to fabricate photodoped SWCNT sheets (Fig. 2a).

The Seebeck coefficient and electrical conductivity of the SWCNT sheets (thickness: 1.2 µm) were measured in a helium atmosphere (Figs. 2b and 2c). The pristine SWCNT sheets had a positive Seebeck coefficient (43.2 ± 1.5 µV/K), indicative of p-type behavior (Fig. 2b, black dot). After PBG1 doping using solutions with different PBG1 concentrations, these sheets still showed a positive Seebeck coefficient (22.3 to 26.5 µV/K), but the value was lower than that of the pristine SWCNT sheet, suggesting mild electron transfer from PBG1 to the SWCNTs (Fig. 2b, blue dots). Conversely, after UV irradiation, the Seebeck coefficient became negative (−33.1 to −37.9 µV/K), suggesting successful photoinduced n-doping (Fig. 2b, red dots). The electrical conductivities of the PBG1-doped SWCNT sheets were slightly lower than that of the pristine sheet, and relatively unaffected by the PBG1 concentration (Fig. 2c, blue dots). After UV irradiation, the electrical conductivity markedly increased and rose with increasing PBG1 concentration (Fig. 2c, red dots). These results support the finding that PBG1 doping results in weak electron transfer to the p-type SWCNTs before UV irradiation, while UV irradiation injects numerous electrons into the SWCNTs via the photochemical reaction of PBG1.

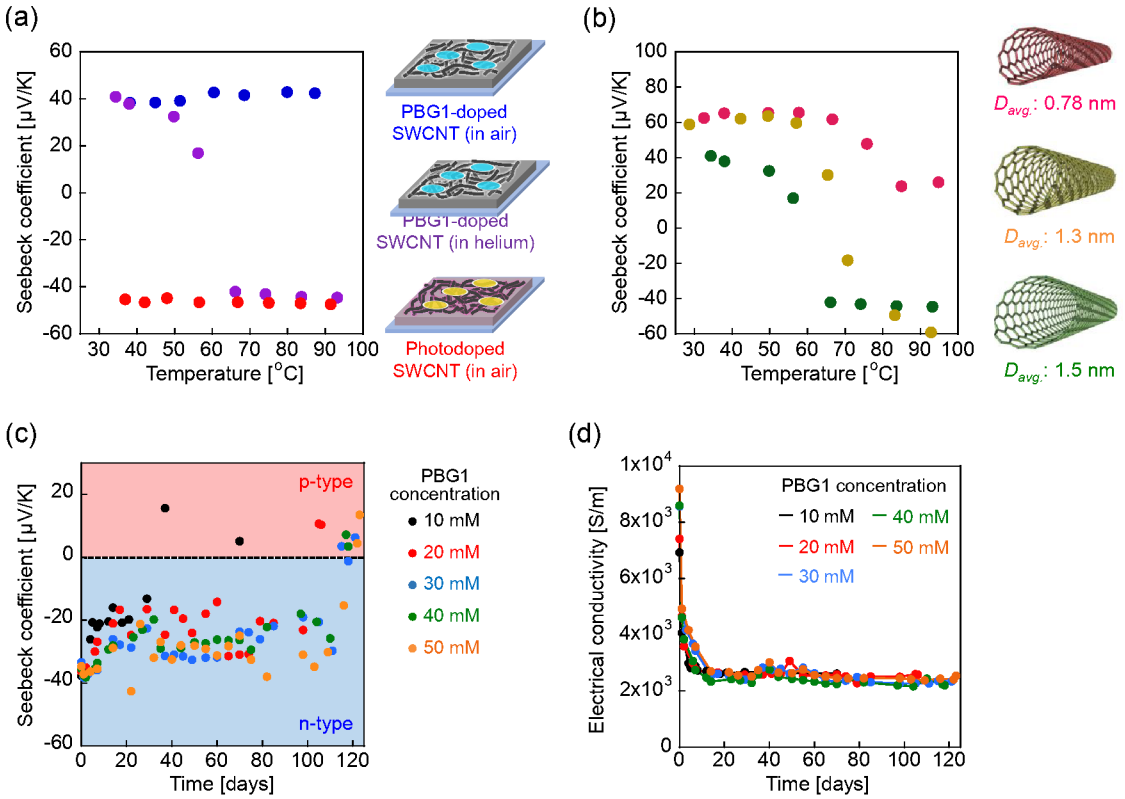

Fig. 3 (a) Temperature dependence of Seebeck coefficient for PBG1-doped SWCNT sheets before (blue) and after (red) UV irradiation, as measured in air, and PBG1-doped SWCNT sheets in a helium atmosphere (purple). (b) Temperature dependence of Seebeck coefficient for PBG1-doped SWCNTs with average diameters ($D_{avg.}$) of 1.5 (green), 1.3 (yellow), and 0.78 nm (red). (c) Time dependence of Seebeck coefficient and (d) electrical conductivity in air for photodoped SWCNT sheets prepared using 10 (black), 20 (red), 30 (blue), 40 (green), and 50 (orange) mM PBG1 solutions.

We also investigated the UV irradiation time and SWCNT sheet thickness dependencies of photoinduced doping (doped with a 30 mM PBG1 solution). Both the Seebeck coefficient and electrical conductivity remained stable when the irradiation time was extended from 1 to 10 min (Fig. 2d), indicating that a 1 min irradiation time was sufficient to complete n-doping (see also Fig. S3†). In terms of the thickness dependency, the photoinduced electron doping was completed within 1 min for sheets up to 5 μm thick. However, for 14 μm thick sheets, the Seebeck coefficient was still positive after 5 min of irradiation, and only became negative (−33.2 μV/K) after 30 min of irradiation (Fig. 2e). These findings suggest that PBG1-based photoinduced doping is more efficient than previous methods using DMBI-Ox, which does not proceed in SWCNTs thicker than 7 μm.[36]

3.2 Thermal and Air Stability of Photodoped SWCNT

In terms of thermal stability, the Seebeck coefficient of the SWCNT sheets doped with a 30 mM PBG1 solution (PBG1-doped SWCNT sheets) fell sharply upon heating from 50 to 60 °C under a helium atmosphere (Fig. 3a, purple dots). We consider that thermally activated electron doping proceeds from the HOMO of PBG1 to the conduction band of the SWCNTs since the highest occupied molecular orbital (HOMO) energy level of PBG1 is higher than that of the semiconducting SWCNTs. On cooling cycle, the Seebeck coefficient of the PBG1-doped SWCNT sheets was remained negative (ca. −40 μV/K) in a helium atmosphere (Fig. S4†). However, after aging the sheets in air for 24 hours, the Seebeck coefficient returned to a positive value (ca. 40 μV/K, Fig. S5†). These results clearly indicate that the PBG1-based thermal doping was irreversible in inert condition but reversible in atmospheric condition. Therefore, thermal doping method is not suitable for the practical TEG used under atmospheric condition. Interestingly, we found that the Seebeck coefficients of the PBG1-doped SWCNT sheets remained positive up to 90 °C when the measurements were carried out in air (Fig. 3a, blue dots). We consider that oxygen molecules attached on the SWCNT surface predominantly acted as p-dopant even in the presence of PBG1 under atmospheric condition. On the other hand, the photodoped SWCNT sheets showed negative Seebeck coefficients up to 95 °C even under atmospheric condition (Fig. 3a, red dots). Thermal stability of the electrical conductivity for the photodoped SWCNT sheets were also confirmed in this temperature range (Fig. S6†). Such high air stability is beneficial for the practical TEGs application.

To further study the thermally activated electron doping of PBG1-doped SWCNTs observed in a helium atmosphere (Fig. 3a), the Seebeck coefficients of SWCNTs with different

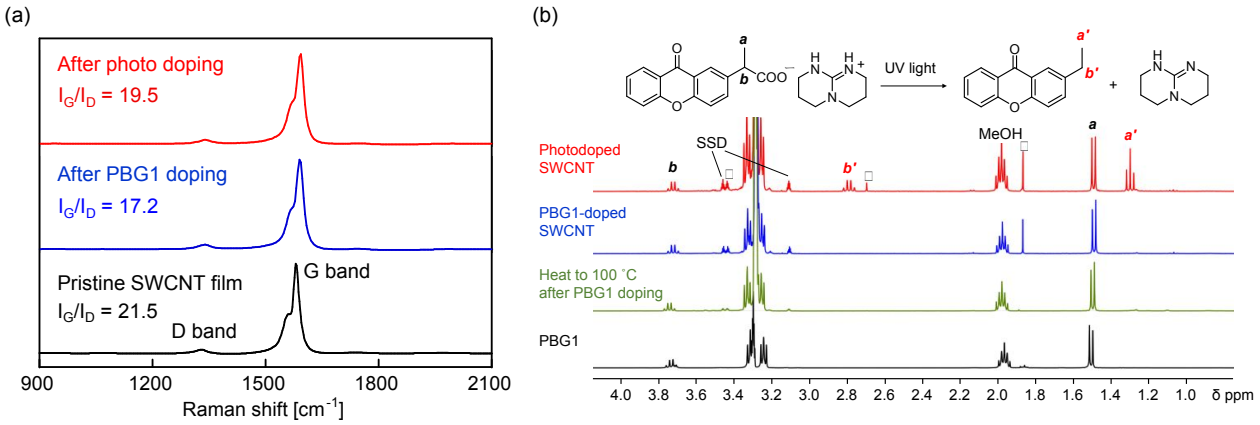

Fig. 4 (a) Raman spectra of pristine, PBG1-doped, and photodoped SWCNT sheets. (b) ^{1}H NMR spectra of PBG1 (black), PBG1-doped SWCNT sheet after heating at 100 °C (green), and PBG1-doped SWCNT sheets before (blue) and after (red) UV irradiation in MeOH-d_3 solution. Peaks marked with asterisks remain unattributed.

diameters, which have different conduction band levels, were measured. The Seebeck coefficient started decreasing from ca. 50, 66, and 71 °C for SWCNTs with diameters of 1.5, 1.3, and 0.78 nm, respectively (Fig. 3b). Given that SWCNTs with larger diameters have lower conduction band energy levels,[45] the predominant doping for larger-diameter SWCNTs aligns with our hypothesis that thermal doping involves electron transfer from the HOMO of PBG1 to the conduction band of the SWCNTs. For the electrical conductivity, decrease and then increase of the values were observed for the PBG1-doped SWCNT having average diameter of 1.5 and 1.3 nm (Fig. S7†), corresponding to the change from p-type to n-type. On the other hand, only the monotonical decrease was observed for PBG1-doped SWCNT with an average diameter of 0.78 nm, corresponding to the decrease of the Seebeck coefficient without involving p-type to n-type transition.

To study their air stability of the photodoped SWCNT sheets (1 min irradiation), the Seebeck coefficient and electrical conductivity were monitored for 120 days (Figs. 3c and 3d). As shown in Fig. 3c, the n-type nature was maintained for longer as the doping concentration increased, reaching over 100 days of air stability when the 30 mM dopant solution was used. On the other hand, irrespective of the doping concentration, the electrical conductivity gradually decreased over the first 20 days, after which it stabilized (Fig. 3d). Similar changes were also observed for the power factor (Fig. S8†). These trends are consistent with previous reports.[22] The reasons for the difference in behavior between the Seebeck coefficient and electrical conductivity remain unclear, but we hypothesize that semiconducting SWCNTs mainly influenced Seebeck coefficient and metallic SWCNTs predominantly influence electric conductivity, where metallic SWCNT might be more sensitive to oxidation by water and/or oxygen due to the presence of continuous density of state.

3.3 Structural Characterization of Photodoped SWCNT

We further explored the thermally activated electron transfer using PBGs with various cation structures (PBG2, PBG3, and PBG4 in Fig. S9†). For all samples, we used 30 mM PBG solutions to prepare PBG-doped SWCNT sheets and measured their electrical conductivities and Seebeck coefficients at 30 °C in a helium atmosphere. The PBG2- and PBG3-doped SWCNT sheets had negative Seebeck coefficients, indicating the spontaneous p–n transformation of the SWCNTs through electron transfer from the PBGs. Conversely, the Seebeck coefficient of the PBG4-doped SWCNT sheet remained positive. We theorize that the extended π-conjugated system in the guanidinium ion structures of the cation moieties in PBG2 and PBG3 increased the HOMO energy level compared to that of PBG1, resulting in the spontaneous electron doping (Fig. S10†). In contrast, because the borate anion in PBG4 is chemically stable, the HOMO energy level for PBG4 is lower than the conduction band of the SWCNTs. These findings provide guidance for the design requirements of PBGs for photoinduced electron doping.

We conducted Raman spectroscopy to characterize the surface structures of the SWCNT sheets before and after photoinduced doping (Fig. 4a). The D-band at 1330 cm^{-1} and G-band at 1581 cm^{-1} originate from sp3 defects of the carbon atoms and stretching vibrations in the ring structures, respectively; therefore, the relative intensity of the D-band to the G-band (G/D ratio) can be used to assess crystallinity of SWCNTs. The G/D ratios for the PBG1-doped (17.2) and photodoped (19.5) SWCNTs sheets were similar to that of the pristine SWCNT sheet (21.5), indicating that sp^3 defects did not form after photoinduced doping.

Further characterization of the chemical structure of PBG1 on the SWCNTs was achieved through ^{1}H NMR spectroscopy. The PBG1-doped and photodoped SWCNT sheets (1 mW/cm^2, 20 min irradiation) were immersed in deuterium methanol (MeOH-d_3) to extract the dopant, and the resulting solutions were then studied (Fig. 4b). The ^{1}H NMR spectrum of the solution extracted from a heat-treated (100 °C, 60 min) PBG1-doped SWCNT sheet was also measured to assess the thermal stability of PBG1 on the SWCNTs. In the spectrum of the photodoped SWCNT sheet (Fig. 4b, red line), new peaks appeared at 2.8 and 1.3 ppm, which were assigned to the ethyl group produced by

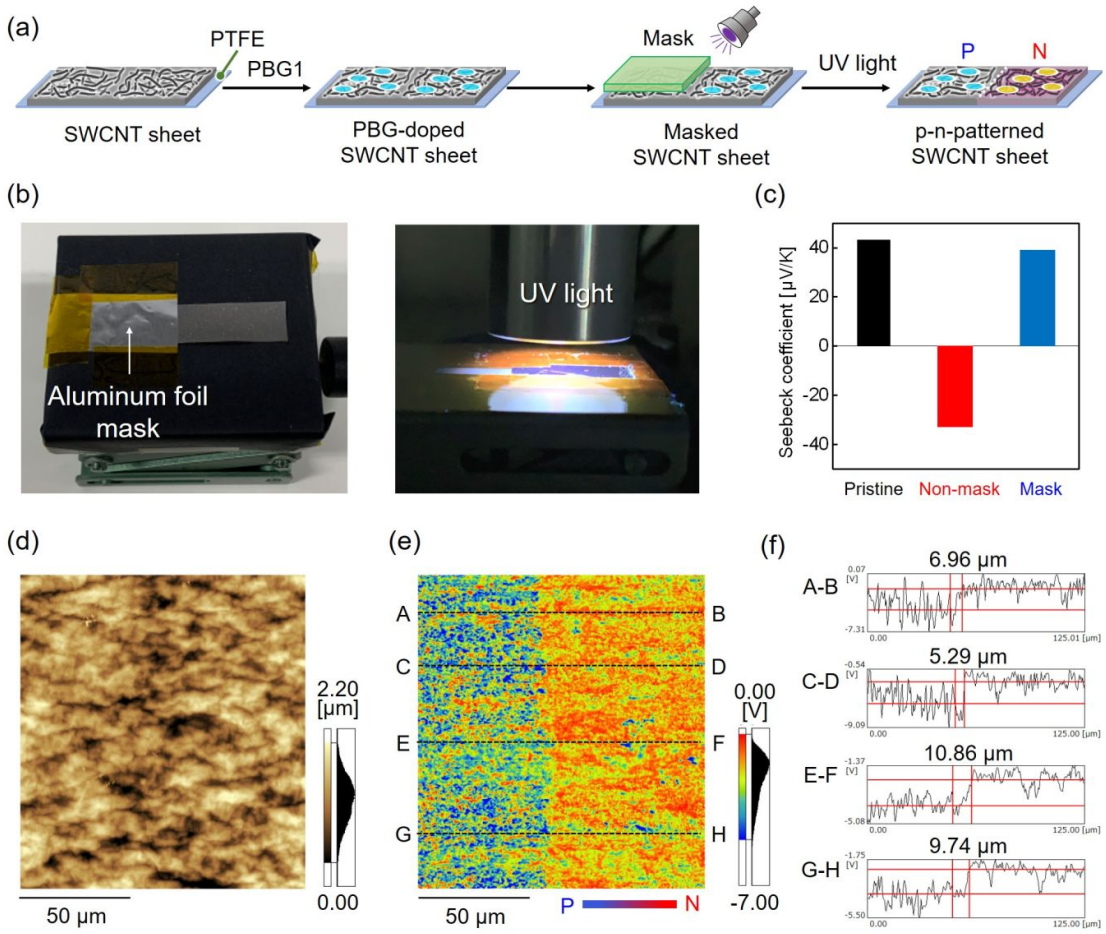

Fig. 5 (a) p–n Patterning of SWCNT sheets by photoirradiation using aluminum foil mask. (b) Photographs of masked SWCNT sheet and UV irradiation process. (c) Seebeck coefficient of pristine (black), non-masked (red), and masked (blue) SWCNT sheets, as measured at room temperature in air. (d) Height profile and e surface potential of the p–n interface in a 125 × 125 μm region (red: positive potential, blue: negative potential). (f) Cross-sectional surface potential profiles of the p–n junction interface in regions A–B, C–D, E–F, and G–H.

the photoconversion of PBG1, the spectra of the PBG1-doped (Fig. 4b, blue line) and heat-treated (Fig. 4b, green line) PBG1-doped SWCNT sheets showed no such peaks. This indicates that thermally induced electron doping from PBG1 did not occur at 25 °C or even 100 °C in air. Despite a photoconversion efficiency of only 38% for the photodoped SWCNT sheets (Fig. S11†), as calculated from the intensity ratio of the peaks of ethyl protons at 3.7 and 2.8 ppm, the electrical conductivity of the photodoped SWCNT sheets remained high (8730 S/m). Notably, the electrical conductivity was comparable to that of the photodoped SWCNT sheets irradiated at 50 mW/cm^2 for 1 min (9403 S/m). This suggests that the electron transfer efficiency from TBD to the SWCNTs is very high and explains why the spontaneous reaction occurs.

3.4 p-n Patterning of SWCNT Sheets

To fabricate SWCNT sheets with p–n patterns, we employed an aluminum foil photomask to cover half of each PBG1-doped SWCNT sheet, and then exposed them to UV irradiation (Figs. 5a and 5b). (This and all the following experiments used a 30 mM PBG1 doping solution.) After irradiation, we separated the exposed and masked sections of the SWCNT sheets and measured their Seebeck coefficients to confirm the success of the doping process (Fig. 5c). The exposed area had a Seebeck coefficient of −32.7 μV/K, while that of the masked area was 38.8 μV/K, corroborating that photoinduced electron doping occurred selectively in the exposed area.

The patterning resolution of the p–n patterns on the SWCNT sheets was evaluated using Kelvin force microscopy (KFM).[35] Figs. 5d and 5e show the height profile and potential difference image, respectively, at the p–n interface in the photodoped SWCNT sheet (thickness: 2.3 μm). The root mean square roughness was approximately 2 μm in both the exposed and masked areas. However, the potential of the irradiated area became negative after irradiation, and a clear potential boundary became evident. In KFM measurements, the electrostatic force between the sample surface and cantilever is monitored by applying electric current through the cantilever; therefore, the change in polarity indicates the difference in the electrical potential between the p- and n-doped areas. Notably,

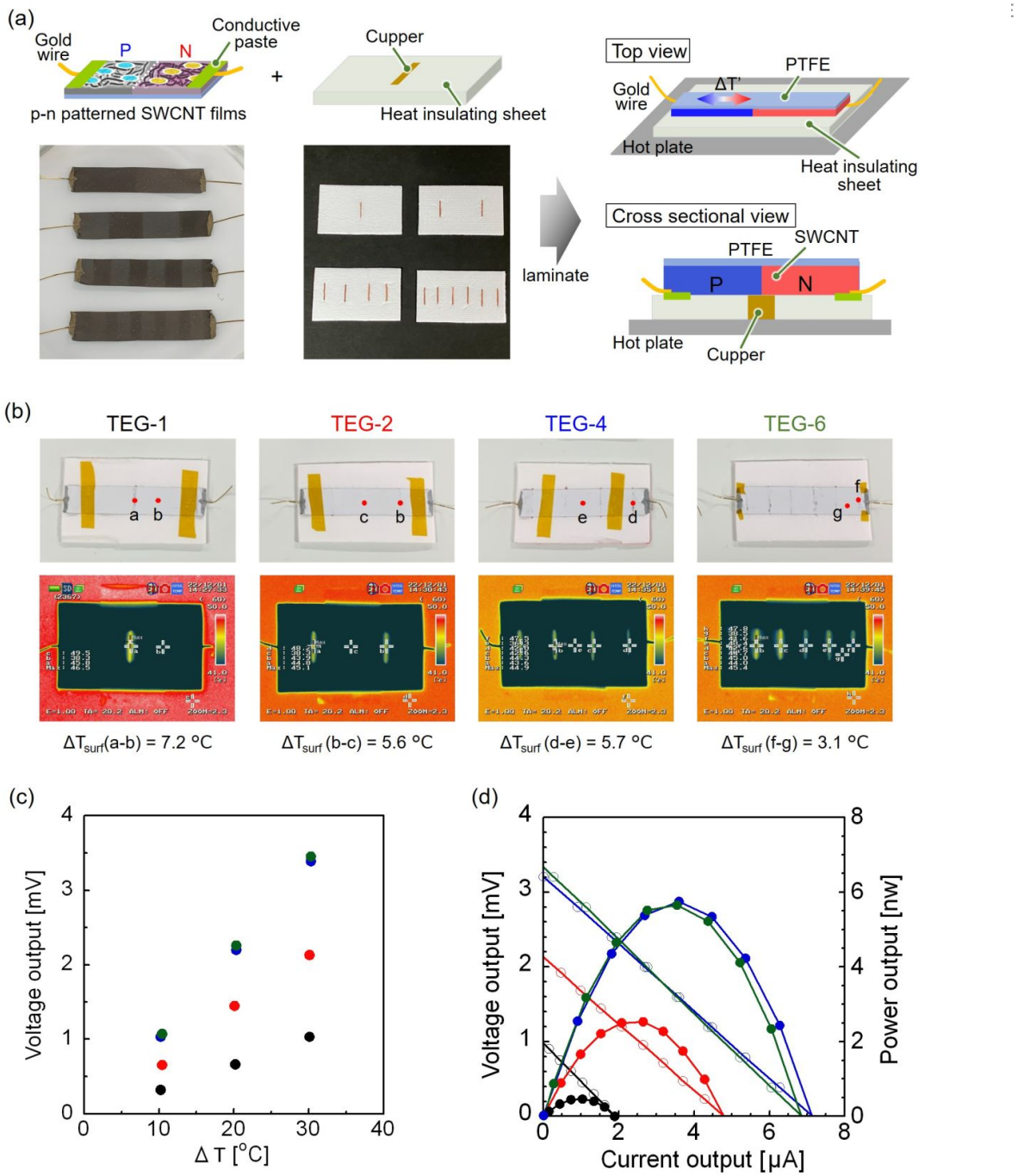

Fig. 6 (a) Fabrication procedure for planar-type TEG device using p–n patterned SWCNT sheet. (b) Photographs (upper panels) and thermal images (lower panels) taken at ΔT_{HP-RT} (the temperature difference between the room and heater temperatures) of 30 °C. The ΔT_{surf} values were calculated as the difference in temperature between two observation points (red points). (c) Plots of V_{OC} for TEG-1 (black), TEG-2 (red), TEG-4 (blue), and TEG-6 (green) as a function of ΔT_{HP-RT}. (d) Voltage output (open circles) and power output (filled circles) for TEG-1 (green), TEG-2 (blue), and TEG-4 (red), and TEG-6 (green) as a function of the current output at ΔT_{HP-RT} = 30 °C.

the region between the p-type (38.8 μV/K) and n-type (−32.7 μV/K) regions was only approximately 10 μm wide (Fig. 5f), indicating that a high-resolution patterning was achieved. The patterning resolution was comparable to that of the plasma treatment system (~5 μm).[35]

3.5 Fabrication of Planar TEGs

Finally, we constructed planar-type TEG devices from SWCNT sheets with one, two, four, or six p–n sequences, denoted as TEG-1, TEG-2, TEG-4, and TEG-6, respectively. The SWCNT sheets were patterned by photoinduced doping using slit masks. A temperature gradient was generated in the in-plane direction of the planar SWCNT-based TEGs by limiting the heating area to the p–n boundaries.[23,36] Copper rods were attached as thermal conductors at the p–n boundaries, while

the other areas were insulated with a thermal insulating sheet (Fig. 6a). The resistances of the sheets (423 – 447 Ω) without any patterns were increased after PBG1 doping (1026 - 1056 Ω), but their resistances were decreased (743 – 836 Ω) after photodoping due to photoinduced electron injection (Table S1†). In addition, the resistance of the photodoped SWCNT sheets having p-n patterns was increased as the number of the patterns increased because of the formation of p-n junctions.[35] On the other hand, the resistance of the TEGs was umch lower than that of the photodoped SWCNT sheets and independent on the number of patterns. We consider that the electrical current at the junctions went through the copper rods attached at the junctions rather than p-n boundary. Photographs of TEG-1, TEG-2, TEG-4, and TEG-6 are shown in the top panels of Fig. 6b. The TEG devices were then placed on a hot plate, and their surface temperatures were monitored using a thermal camera, as shown in the lower panels of Fig. 6b. The hot plate temperature was manipulated to maintain a specific temperature difference between the room and hot plate temperatures (ΔT_{HP-RT}). When ΔT_{HP-RT} was 30 °C, the temperature differences between the p–n boundaries and the halfway points between two p–n boundaries (ΔT_{surf}) were 7.2, 5.6, 5.7, and 3.1 °C for TEG-1, TEG-2, TEG-4, and TEG-6, respectively (Fig. 6b). The lower ΔT_{surf} values for larger p–n patterns were caused due to in-plane heat diffusion.

We calculated the open-circuit voltages using Eq. (1), where $\Delta T = \Delta T_{surf}$ and S_P and S_N (at 50 °C) were 38.8 and −32.7 μV/K, respectively. The calculated open-circuit voltages for TEG-1, TEG-2, TEG-4, and TEG-6 were 0.515, 0.801, 1.63, and 1.33 mV, respectively. Fig. 6c shows the calculated V_{OC} values at ΔT_{HP-RT} = 10, 20, and 30 °C, demonstrating linear increases in V_{OC} with ΔT_{HP-RT}. The measured V_{OC} values at ΔT_{HP-RT} = 30 °C for TEG-1, TEG-2, TEG-4, and TEG-6 were 1.03, 2.13, 3.34, and 3.45 mV, respectively. These values are higher than the values calculated using ΔT_{surf}, suggesting that the temperature difference inside the sheets is greater than that at the surface. Fig. 6d shows the voltage and power output profiles of the TEGs as a function of the current output on a hot plate at ΔT_{HP-RT} = 30 °C. The power outputs of TEG-1, TEG-2, TEG-4, and TEG-6 were 0.47, 2.53, 5.75, and 5.65 nW, respectively. These findings demonstrate the potential utility of the photodoped SWCNT sheets for wearable thermoelectric applications. Durability tests including cycling tests and stability tests are undergoing to estimate the applicability in the practical. Although this paper focuses on p-n patterned SWCNT sheets for TEG, they can actually be applied to other electronic devices such as diodes and transistors. We hope that this technology will be used as a method to fabricate a variety of electronic devices in the future.

4. Conclusion

Through the use of PBG1 as a photoinduced electron dopant, we successfully achieved the photoinduced n-doping of SWCNT sheets. The conversion of PBG1-doped SWCNT sheets (p-type) to n-type was facilitated through a 1 min UV irradiation treatment, highlighting the efficiency of electron transfer from the photogenerated PBG1 cations to the SWCNTs. Furthermore, because PBG1 formed stable cations after doping, the n-type SWCNT sheets exhibited impressive air stability, exceeding 100 days. Atmospheric oxygen played a crucial role in maintaining the p-type nature of the PBG1-doped SWCNT sheets up to 90 °C. We successfully created alternating p–n patterned SWCNTs by UV irradiation of PBG1-doped SWCNT sheets using a photomask with a patterning resolution of less than 10 μm. Leveraging photodoped SWCNT sheets with one, two, four, and six p–n sequences, we fabricated planar-type TEGs. The TEG with six p–n sequences (TEG-6) achieved an open-circuit voltage and maximum power output of 3.45 mV and 5.65 nW, respectively, at a 30 °C temperature difference between the hot plate and room temperature.

Author Contributions

N.T. and T.F. designed the study and wrote the manuscript. N.T., M.Y., and E. H. performed the experiments. M.Y., I.Y., A.H., and E.H. analyzed the results and contributed to the discussion of the manuscript. All the authors discussed the results and revised the manuscript.

Conflicts of interest

There are no conflicts to declare.

Acknowledgements

This work was supported by KAKENHI (Nos. 18H01816, 19K23633, and 20K15355) and bilateral programs (No. AJ190078) of the Japan Society for the Promotion of Science (JSPS), the Nanotechnology Platform Project from the Ministry of Education, Culture, Sports, Science, and Technology (MEXT), Japan, and the Core Research for Evolutional Science and Technology (CREST) (No. JPMJCR19Q5), and ACT-X (no. JPMJAX21KB) of the Japan Science and Technology Agency (JST). We also acknowledge Shimadzu Corporation for the KFM measurement of the p–n patterned SWCNT sheet.

Notes and references

1 H. Hatcher, *Nat. Rev. Mater.* 2022, **7**, 256.
2 R. Liu, Z. L. Wang, K. Fukuda and T. Someya, *Nat. Rev. Mater.* 2022, **7**, 870.
3 Y. Wang, T. Guo, Z. Tian, K. Bibi, Y. Z. Zhang and H. N. Alshareef, *Adv. Mater.* 2022, **34**, e2108560.
4 N. Sezer and M. Koç, *Nano Energy* 2021, **80**.
5 C. Jiang, X. Li, S. W. M. Lian, Y. Ying, J. S. Ho and J. Ping, *ACS Nano* 2021, **15**, 9328.
6 Y. Jia, Q. Jiang, H. Sun, P. Liu, D. Hu, Y. Pei, W. Liu, X. Crispin, S. Fabiano, Y. Ma and Y. Cao, *Adv. Mater.* 2021, **33** e2102990.
7 M. Massetti, F. Jiao, A. J. Ferguson, D. Zhao, K. Wijeratne, A. Wurger, J. L. Blackburn, X. Crispin and S. Fabiano, *Chem. Rev.* 2021, **121** 12465.
8 M. Hong, M. Li, Y. Wang, X. L. Shi and Z. G. Chen, *Adv. Mater.* 2023, **35** e2208272.
9 X. L. Shi, J. Zou, and Z. G. Chen, *Chem. Rev.* 2020, **120**, 7399.
10 H. Jin, J. Li, J. Iocozzia, X. Zeng, P. C. Wei, C. Yang, N. Li, Z. Liu,

J. H. He, T. Zhu, J. Wang, Z. Lin, and S. Wang, *Angew. Chem. Int. Ed. Engl.* 2019, **58**, 15206.
11 V. Karthikeyan, J. U. Surjadi, X. Li, R. Fan, V. C. S. Theja, W. J. Li, Y. Lu, and V. A. L. Roy, *Nat. Commun.* 2023, **14**, 2069.
12 B. Lee, H. Cho, K. T. Park, J. S. Kim, M. Park, H. Kim, Y. Hong and S. Chung, *Nat. Commun.* 2020, **11**, 5948.
13 M. H. Jeong, K. C. Kim, J. S. Kim, and K. J. Choi, *Adv. Sci. (Weinh)* 2022, **9**, e2104915.
14 M. M. Mallick, L. Franke, A. G. Rösch and U. Lemmer, *ACS Energy Lett.* 2020, **6**, 85.
15 Y. Jiang, J. Dong, H. L. Zhuang, J. Yu, B. Su, H. Li, J. Pei, F. H. Sun, M. Zhou, H. Hu, J. W. Li, Z. Han, B. P. Zhang, T. Mori and J. F. Li, *Nat. Commun.* 2022, **13**, 6087.
16 Y. Wang, Z. Zhou, J. Zhou, L. Shao, Y. Wang and Y. Deng, *Adv. Energy Mater.* 2021, **12**.
17 J. L. Blackburn, A. J. Ferguson, C. Cho and J. C. Grunlan, *Adv. Mater.* 2018, **30**, 1704386.
18 N. Komatsu, Y. Ichinose, O. S. Dewey, L. W. Taylor, M. A. Trafford, Y. Yomogida, G. Wehmeyer, M. Pasquali, K. Yanagi and J. Kono, *Nat. Commun.* 2021, **12**, 4931.
19 M. Rdest and D. Janas, *Materials (Basel)* 2020, **14**, 65.
20 C. Yu, A. Murali, K. Choi and Y. Ryu, *Energy Environ. Sci.* 2012, **5**, 9481.
21 K. S. Mistry, B. A. Larsen, J. D. Bergeson, T. M. Barnes, G. Teeter, C. Engtrakul, and J. L. Blackburn, *ACS Nano*, 2011, **5**, 3714.
22 Y. Nakashima, R. Yamaguchi, F. Toshimitsu, M. Matsumoto, A. Borah, A. Staykov, M. S. Islam, S. Hayami and T. Fujigaya, *ACS Appl. Nano Mater.* 2019, **2**, 4703.
23 R. Yamaguchi, T. Ishii, M. Matsumoto, A. Borah, N. Tanaka, K. Oda, M. Tomita, T. Watanabe and T. Fujigaya, *J. Mater. Chem. A* 2021, **9**, 12188.
24 Y. Nakashima, N. Nakashima and T. Fujigaya, *Synthetic Metals* 2017, **225**, 76.
25 H. Wang, P. Wei, Y. Li, J. Han, H. R. Lee, B. D. Naab, N. Liu, C. Wang, E. Adijanto, B. C. Tee, S. Morishita, Q. Li, Y. Gao, Y. Cui and Z. Bao, *Proc. Natl. Acad. Sci. U. S. A.* 2014, **111**, 4776.
26 Y. Wang, Q. Li, J. Wang, Z. Li, K. Li, X. Dai, J. Pan and H. Wang, *Nano Energy* 2022, **93**, 106804.
27 Y. Nonoguchi, M. Nakano, T. Murayama, H. Hagino, S. Hama, K. Miyazaki, R. Matsubara, M. Nakamura and T. Kawai, *Adv. Funct. Mater.* 2016, **26**, 3021.
28 D. Suzuki, Y. Ochiai, Y. Nakagawa, Y. Kuwahara, T. Saito and Y. Kawano, *ACS Appl. Nano Mater.* 2018, **1**, 2469.
29 S. Horike, Q. Wei, K. Akaike, K. Kirihara, M. Mukaida, Y. Koshiba and K. Ishida, *Nat. Commun.* 2022, **13**, 3517.
30 G. Wu, Z. G. Zhang, Y. Li, C. Gao, X. Wang and G. Chen, *ACS Nano* 2017, **11**, 5746.
31 Y. Zheng, Q. Zhang, W. Jin, Y. Jing, X. Chen, X. Han, Q. Bao, Y. Liu, X. Wang, S. Wang, Y. Qiu, C.-a. Di and K. Zhang, *J. Mater. Chem. A* 2020, **8**, 2984.
32 T. Sun, B. Zhou, Q. Zheng, L. Wang, W. Jiang and G. J. Snyder, *Nat. Commun.* 2020, **11**, 572.
33 J. Choi, Y. Jung, S. J. Yang, J. Y. Oh, J. Oh, K. Jo, J. G. Son, S. E. Moon, C. R. Park and H. Kim, *ACS Nano* 2017, **11**, 7608.
34 W. Zhou, Q. Fan, Q. Zhang, L. Cai, K. Li, X. Gu, F. Yang, N. Zhang, Y. Wang, H. Liu, W. Zhou and S. Xie, *Nat. Commun.* 2017, **8**, 14886.
35 X. Dai, Y. Wang, K. Li, G. Li, J. Wang, X. Sun, L. Zhang and H. Wang, *ACS Energy Lett.* 2021, **6**, 4355.
36 N. Tanaka, T. Ishii, I. Yamaguchi, A. Hamasuna and T. Fujigaya, *J. Mater. Chem. A* 2023, **11**, 6909.
37 N. Zivic, P. K. Kuroishi, F. Dumur, D. Gigmes, A. P. Dove and H. Sardon, *Angew. Chem. Int. Ed. Engl.* 2019, **58**, 10410.
38 X. Sun, J. P. Gao and Y. Wang, *J. Am. Chem. Soc.* 2008, **130**, 8130.
39 C. Ley, A. Siedel, T. Bertaux, C. Croutxe-Barghorn and X. Allonas, *Angew. Chem. Int. Ed. Engl.* 2023, **262**, e202214784.
40 J. Baltazar, H. Sojoudi, S. A. Paniagua, S. Zhang, R. Lawson, S. R. Marder, S. Graham, L. M. Tolbert and C. L. Henderson, *Adv. Funct. Mater.* 2014, **24**, 5147.
41 B. K. Keitz, C. J. Yu, J. R. Long and R. Ameloot, *Angew. Chem. Int. Ed. Engl.* 2014, **53**, 5561.
42 Q.S. Wei, M. Mukaida, K. Kirihara, Y. Naitoh and T. Ishida, *ACS Appl. Mater. Interfaces*, 2016, **8**, 2054.
43 K. Noda, S. Kikuchi, N. Ikumura, D. Shiota, M. Furutani and K. Arimitsu, *J. Photopolym. Sci. Technol.* 2019, **32**, 265.
44 K. Arimitsu and R. Endo, *Chem. Mater.* 2013, **25**, 4461 (2013).
45 Y. Hirana, G. Juhasz, Y. Miyauchi, S. Mouri, K. Matsuda and N. Nakashima, *Sci. Rep.* 2013, **3**, 2959.